Silica Nanoparticles at Interfaces Modulated by Amphiphilic Polymer and Surfactant

Camila Alves de Rezende,[†,‡] Lay-Theng Lee,*[,†] and Fernando Galembeck[‡]

Laboratoire Léon Brillouin, CEA-Saclay, 91191 Gif-sur-Yvette Cedex, France, and Instituto de Química, Universidade Estadual de Campinas, P.O. Box 6154, 13083-970 Campinas SP-Brazil

Received February 14, 2008. Revised Manuscript Received April 17, 2008

The interfacial behavior of silica nanoparticles in the presence of an amphiphilic polymer poly(*N*-isopropylacrylamide) (PNIPAM) and an anionic surfactant sodium dodecyl sulfate (SDS) is studied using neutron reflectivity. While the nanoparticles do not show any attraction to hydrophilic and hydrophobic surfaces in pure water, presence of the amphiphilic polymer induces significant adsorption of the nanoparticles at the hydrophobic surface. This interfacial behavior is activated due to interaction of the nanoparticles with PNIPAM, the amphiphilic nature of which leads to strong adsorption at a hydrophobic surface but only weak interaction with a hydrophilic surface. The presence of SDS competes with nanoparticle−PNIPAM interaction and in turn modulates the interfacial properties of the nanoparticles. These adsorption results are discussed in relation to nanoparticle organization templated by dewetting of charged polymer solutions on a solid substrate. Our previous studies showed that nanoparticle assembly can be induced to form complex morphologies produced by dewetting of the polymer solutions, such as a polygonal network and long-chain structures. This approach, however, works on a hydrophilic substrate but not on a hydrophobic substrate. These observations can be explained in part by particle−substrate interactions revealed in the present study.

Introduction

Nanoparticle self-assembly is an important process for the production of nanometric structures that can be used in electronic[1] and magnetic[2] devices, photonic crystals,[3] films with antistatic properties,[4] biotechnology,[5,6] and other applications.[7] In order for organized structures to have functional applications, it is necessary to direct the self-assembly process to obtain open and complex arrays. Different strategies have been proposed with this aim: use of prepatterned substrates,[2,8,9] polymeric molecules,[10] copolymer microphases,[11–14] carbon nanotubes,[15,16] and biotemplates such as DNA molecules,[17] proteins,[18] bacterial,[19] and viral structures.[20]

Other techniques like microcontact printing,[21–23] vapor deposition,[24] monolayer chemical templates,[25] and capillary force lithography[26] have been used to promote inhomogeneities on substrates to organize particles. Other methods emphasize capillary forces between particles during liquid evaporation in thin liquid films.[27] Nagayama[28] and Kralchevsky[29] applied this method to protein systems, while Sehgal and collaborators applied it to ultrathin dewetting polystyrene films using chemically patterned substrates by microprinting of progressively narrower arrays of stripes.[21] Zhang and collaborators have employed substrates with regular patterns of self-assembled monolayers produced by microcontact printing with octadecyltrichlorosilane to direct the dewetting process in thin polystyrene films forming patterns of micrometer scale.[22]

Self-assembly together with nanomanipulation and chemical synthesis are the three important approaches for producing nanostructures and are therefore key processes for nanotechnology development. The reported methods to control nanoparticle self-assembly forming open complex domains also include the use of electric force fields,[1,30] fluid-assisted dewetting[31] and formation

* To whom correspondence should be addressed. E-mail: lay-theng.lee@cea.fr.

[†] Laboratoire Léon Brillouin.

[‡] Instituto de Qu´mica.

(1) Hermanson, K. D.; Lumsdon, S. O.; Williams, J. P.; Kaler, E. W.; Velev, O. D. *Science* **2001**, *294*, 1082.

(2) An, L. J.; Li, W.; Nie, Y. R.; Xie, B.; Li, Z. Q.; Zhang, J. H.; Yang, B. *J. Colloid Interface Sci.* **2005**, *288*, 503.

(3) Xu, X. L.; Friedman, G.; Humfeld, K. D.; Majetich, S. A.; Asher, S. A. *Adv. Mater.* **2001**, *13*, 1681.

(4) Wakabayashi, A.; Sasakawa, Y.; Dobashi, T.; Yamamoto, T. *Langmuir* **2006**, *22*, 9260.

(5) Doyle, P. S.; Bibette, J.; Bancaud, A.; Viovy, J. L. *Science* **2002**, *295*, 2237.

(6) Huwiler, C.; Halter, M.; Rezwan, K.; Falconnet, D.; Textor, M.; Voros, J. *Nanotechnology* **2005**, *16*, 3045.

(7) Haken, H. *Information and self-organization: a macroscopic approach to complex systems*; Springer-Verlag: Berlin, 2000; 222p

(8) Kumar, A.; Whitesides, G. M. *Appl. Phys. Lett.* **1993**, *63*, 2002.

(9) Aizenberg, J.; Braun, P. V.; Wiltzius, P. *Phys. Rev. Lett.* **2000**, *84*, 2997.

(10) Burghard, M.; Philipp, G.; Roth, S.; Von Klitzing, K. *Appl. Phys. A* **1998**, *67*, 591.

(11) Cheng, J. Y.; Ross, C. A.; Thomas, E. L.; Smith, H. I.; Vancso, G. J. *Adv. Mater.* **2003**, *15*, 1599.

(12) Zehner, R. W.; Sita, L. R. *Langmuir* **1999**, *15*, 6139.

(13) Hamley, I. W. *Nanotechnology* **2003**, *14*, 39.

(14) Park, C.; Yoon, J.; Thomas, E. L. *Polymer* **2003**, *44*, 6725.

(15) Jiang, K. Y.; Eitan, A.; Schadler, L. S.; Ajayan, P. M.; Siegel, R. W.; Grobert, N.; Mayne, M.; Reyes-Reyes, M.; Terrones, H.; Terrones, M. *Nano Lett.* **2003**, *3*, 275.

(16) Fullam, S.; Cottell, D.; Rensmo, H.; Fitzmaurice, D. *Adv. Mater.* **2000**, *12*, 1430.

(17) Nakao, H.; Shiigi, H.; Yamamoto, Y.; Tokonami, S.; Nagaoka, T.; Sugiyama, S.; Ohtani, T. *Nano Lett.* **2003**, *3*, 1391.

(18) Behrens, S.; Habicht, W.; Wagner, K.; Unger, E. *Adv. Mater.* **2006**, *18*, 284.

(19) He, Y. H.; Yuan, J. Y.; Su, F. Y.; Xing, X. H.; Shi, G. Q. *J. Phys. Chem. B* **2006**, *110*, 17813.

(20) Dujardin, E.; Peet, C.; Stubbs, G.; Culver, J. N.; Mann, S. *Nano Lett.* **2003**, *3*, 413.

(21) Sehgal, A.; Ferreiro, V.; Douglas, J. F.; Amis, E. J.; Karim, A. *Langmuir* **2002**, *18*, 7041.

(22) Zhang, Z. X.; Wang, Z.; Xing, R. B.; Han, Y. C. *Surf. Sci.* **2003**, *539*, 129.

(23) Yoon, B. K.; Huh, J.; Kim, H. C.; Hong, J. M.; Park, C. *Macromolecules* **2006**, *39*, 901.

(24) Zhang, F. J.; Baralia, G.; Boborodea, A.; Bailly, C.; Nysten, B.; Jonas, A. M. *Langmuir* **2005**, *21*, 7427.

(25) Yi, K. C.; Hórvölgyi, Z.; Fendler, J. H. *J. Phys. Chem.* **1994**, *98*, 3872.

(26) Luo, C.; Xing, R.; Han, Y. *Surf. Sci.* **2004**, *552*, 139.

(27) Kralchevsky, P. A.; Nagayama, K. *In Particles at Fluid Interfaces and Membranes; Elsevier: Amsterdam* **2001**, p 503.

(28) Nagayama, K. *Colloids Surf., A* **1996**, *109*, 363.

(29) Kralchevsky, P. A. *Adv. Biophys.* **1997**, *34*, 25.

(30) Yeh, S. R.; Seul, M.; Shraiman, B. I. *Nature* **1997**, *386*, 57.

(31) Dockendorf, C. P. R.; Choi, T. Y.; Poulikakos, D.; Stemmer, A. *Appl. Phys. Lett.* **2006**, *88*, 131903.

10.1021/la8004807 CCC: $40.75
Published on Web 06/12/2008

of nanoyarns at the air−water interface using the Langmuir−Blodgett technique.[32,33] Open arrays of nanoparticles have promising applications in the production of nanoyarns for micro- and nanoelectronic devices. Recent research in this area targets two aspects: (1) assembly of working circuits and (2) making elements capable of promoting electric connections between circuit parts.[34,35]

In our previous work, we proposed a relatively simple approach to promote nanoparticle organization based on patterns formed by dewetting of a thin liquid polymer film from a solid substrate.[36–38] When an aqueous solution of poly(*N*-isopropylacrylamide) (PNIPAM) charged with surfactant aggregates is deposited on mica, it spreads and thins by solvent evaporation until the film reaches a critical thickness where it becomes unstable and dewets the substrate forming different morphologies that include polygonal networks, bicontinuous, and elongated structures.[36] These morphologies thus provide a potential template system for nanoparticle assembly. In this approach, nanoparticles of appropriate size dispersed in the polymer solution are spread in a thin liquid film on a solid substrate. Upon dewetting of the liquid film, the particles are dragged by the receding liquid and confined inside the templates, forming upon drying, well-organized arrays.[37]

The efficiency of the self-assembly process depends on many different parameters that control the particle organization process itself and also on the factors that influence the dewetting of the thin film. Initial results show the importance of the dispersion properties like polymer concentration, surfactant-to-polymer ratio, nanoparticle size, and also of the parameters related to the film like the thickness and the drying temperature that controls the drying rate. More recent studies concentrate on improved control of drying conditions (temperature and relative humidity) and on the influence of the substrate hydrophilicity/hydrophobicity.[38] Well-controlled drying conditions allow formation of large-size organized structures. The nature of the substrate is also shown to be a major factor influencing the pattern formation. On a hydrophilic substrate (mica), it is possible to induce formation of different complex structures such as polygonal networks, bicontinuous structures, and elongated yarns. On more hydrophobic substrates such as crystalline silicon and graphite, this method is not successful; the nanoparticles dry without features of dewetting template.

The effect of substrate hydrophilicity/hydrophobicity on pattern formation highlights the importance of the liquid spreading coefficient for the dewetting process. However, it does not explain the often-observed coexistence of different features, even for complete wetting system, formed by the nanoparticles on the same sample. Clearly, particle−substrate interaction plays an important role. This aspect cannot be elucidated from the above microscopy studies for particles that are deposited and allowed to dry on a substrate.

Particle−substrate interactions can be studied by direct measurement of adsorption properties of the nanoparticles at the different interfaces. In this work, we use neutron reflectivity to investigate the adsorption of silica nanoparticles at hydrophobic and hydrophilic surfaces. The interfacial behaviors of the nanoparticles in polymer and surfactant solutions, and their relation to organization in two dimensions, are reported in this paper. This is the first report to our knowledge concerning nanoparticle adsorption at hydrophobic and hydrophilic interfaces.

Experimental Section

Sample Preparation. The polymer used was an amphiphilic polymer, PNIPAM (M_w = 90k), and the surfactant was sodium dodecyl sulfate (SDS). Stock solutions were prepared using milli-Q (Millipore) water or in D_2O. Samples were prepared by mixing and dilution of these stock solutions. Two series of samples were prepared, one in pure D_2O (scattering length density, Nb = 6.39 10^{-6} Å^{-2}) and one in a mixture of D_2O/H_2O 20:80 (20% D_2O + 80% H_2O by volume, Nb = 0.82 10^{-6}Å^{-2}). This solvent mixture is contrast-matched to the polymer. The final concentration of the polymer solution, $C_p = 10^{-3}$ g/mL. For solutions containing polymer and surfactant, the ratio of the components was kept constant in the present study, and the surfactant concentration $C_s = 10^{-3}$ g/ml ($C_s/C_p = 1$). Nanoparticle dispersions were prepared by incorporating silica nanoparticles in the solution mixtures at concentrations ranging from 0.01% to 6% (by weight). For neutron reflectivity measurements, Ludox LS silica was used (mean diameter $d_p \approx 16$ nm, characterized by neutron scattering.[39] For microscopy imaging, larger particles were more appropriate and Stöber silica was used (mean diameter $d_p \approx 63$ nm, characterized by photon correlation spectroscopy).

Neutron Reflectivity Measurements. Neutron reflectivity experiments were carried out on the time-of-flight neutron reflectometer EROS (Laboratoire Léon Brillouin, CEA-Saclay, France) with wavelengths ranging from 2.5 to 22 Å. Two sets of experiments were conducted at room temperature ($T \approx 22$ °C) at the (1) water−air interface (hydrophobic surface) and (2) solid−liquid interface (hydrophilic surface), using silicon wafers containing an oxidized silica layer. For the liquid−air interface, a Teflon container (15.0 × 5.0 cm^2) was used. The liquid sample was enclosed in an aluminum cell with quartz windows to allow the neutron beam to pass through with minimal absorption. For this set of experiments, the incident angle used was 1.83° ± 0.08° for the pure D_2O series, and 0.63° ± 0.07° for the D_2O/H_2O 20:80 solvent series.

For experiments at the solid−liquid interface, the sample holder was a closed cell with a circular silicon wafer (diameter 4 cm and thickness 0.5 cm) with an oxidized hydrophilic layer (SiO_2) characterized by neutron reflectivity to be about 22 Å. The silicon wafers were washed with Piranha solution (70% H_2SO_4, 30% H_2O_2) and rinsed several times with milli-Q water before use. The incident angle for this set of experiments is 1.32° ± 0.08°, and the solvent used is D_2O. The minimum time for spectrum acquisition was 2 h.

Scanning Electron Microscopy (SEM). About 8 μL of a dilute silica dispersion was deposited on freshly cleaved mica or graphite and allowed to dry under controlled temperature and humidity conditions. The dry samples were coated with Au and Pd using a MED 020 Bal-Tec coater. The sample morphology was analyzed using a scanning microscope (JEOL LV-JSM 6360) operating at 15 keV.

Transmission Electron Microscopy−Electron Energy-Loss Imaging (TEM/ESI). Elemental map distribution analysis was carried out using transmission microscopy coupled to electron energy-loss spectroscopy. About 10 μL of the dilute silica dispersion was deposited on carbon-coated parlodion film supported on 400-mesh copper grid (Ted Pella) and allowed to dry under controlled temperature. A Carl Zeiss CEM 902 transmission electron microscope (80 keV) equipped with a Castaing−Henry energy filter spectrometer and a Proscan Slow Scan CCD camera were used to acquire the images. The spectrometer uses inelastically scattered electrons to form energy-loss spectra and element-specific images.[40] The energy-loss spectra were acquired at 303 eV for carbon and 1090 eV for sodium. Spectral images were acquired around the absorption border

(32) Reuter, T.; Vidoni, O.; Torma, V.; Schmid, G.; Nan, L.; Gleiche, M.; Chi, L.; Fuchs, H. *Nano Lett.* **2002**, *2*, 709.
(33) Chung, S. W.; Markovich, G.; Heath, J. R. *J. Phys. Chem. B* **1998**, *102*, 6685.
(34) Braun, E.; Eichen, Y.; Sivan, U.; Ben-Yoseph, G. *Nature* **1998**, *391*, 775.
(35) Scheibel, T.; Parthasarathy, R.; Sawicki, G.; Lin, X. L.; Jaeger, H.; Linquist, S. L. *PNAS* **2003**, *10*, 4527.
(36) Lee, L. T.; Silva, M. C. V.; Galembeck, F. *Langmuir* **2003**, *19*, 6717.
(37) Lee, L. T.; Leite, C. A. P.; Galembeck, F. *Langmuir* **2004**, *20*, 4430.
(38) Rezende, C. A.; Lee, L. T.; Galembeck, F. *Langmuir* **2007**, *23*, 2824.
(39) Cousin, F. Private communication.
(40) Egerton, R. F. *Electron energy-loss spectroscopy in the electron microscope*; Plenum Press: New York, 1989.

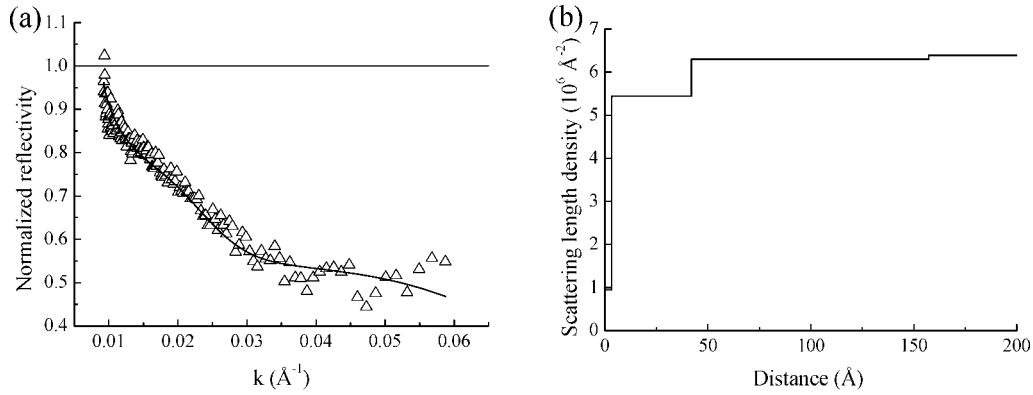

Figure 1. PNIPAM adsorption at the D_2O−air interface: (a) normalized reflectivity, $C_p = 10^{-3}$ g/mL. The continuous line is the best-fit curve using a three-layer model with corresponding profile shown in (b). In this representation, $R/R_F < 1$ is due only to adsorbed polymer layer.

for the element of interest using a three-window method: two below the absorption threshold to determine the background and a third at the absorption band. The elemental map was obtained by subtracting the background from this third image.

Photon Correlation Spectroscopy. Electrophoretic mobility and the effective diameter of the silica particles were measured using Zeta Plus instrument (Brookhaven Instruments) with Bi-MAS software and a solid-state laser (15 mW, $\lambda = 670$ nm) as the radiation source. Dilute dispersions of the sample in distilled water (in 3 mL dust-free acrylic cuvettes) were used for the measurements. Electrophoretic mobility measurements were carried out in 10^{-3} M KCl and the zeta potential values calculated using the Smoluchowski equation. The reported values are the averages of two sample aliquots of 10 measurements each.

Results

Adsorption at Hydrophobic Surface (Air−Water Interface). The first set of experiments was conducted at the air−water interface. Air being apolar, adsorption results obtained at this interface can be considered to represent adsorption behavior on a hydrophobic surface. Two different contrast conditions were used to obtain overall signal, as well as individual signals of the components.

Samples in Pure D_2O. (i) PNIPAM Alone. In this contrast scheme, both PNIPAM and silica nanoparticles contribute to the excess reflectivity signal. The scattering length density of PNIPAM in D_2O is 0.90 10^{-6} Å^{-2}, taking into account 20% labile H exchange with D. The contrast (difference in scattering length density, Nb) in this system is much higher for polymer−solvent ($\Delta Nb = Nb_P - Nb_{D_2O} = 0.90 - 6.39\ 10^{-6}$ Å^{-2} $= -5.49\ 10^{-6}$ Å^{-2}) than for silica nanoparticle−solvent ($\Delta Nb = Nb_{particle} - Nb_{D_2O} = 3.96 - 6.39\ 10^{-6}$ Å^{-2} $= -2.43\ 10^{-6}$ Å^{-2}). Due to the negative sign of ΔNb, the reflectivity due to adsorbed layer is lower compared to that of pure solvent, and the normalized reflectivity, $R/R_F < 1$, where R_F is the reflectivity of the pure solvent. In the presence of solute species, R_F is corrected by considering the total average scattering length density of the bulk phase. Figure 1a shows the normalized reflectivity, R/R_F for PNIPAM in D_2O; in this case, R_F is the reflectivity of pure D_2O. In this representation, deviation of R/R_F from unity is attributed only to the adsorbed polymer layer. The solid line through the experimental points is the fitted curve using a three-layer model—this is a step function model where for each layer, the fitting parameters are thickness and scattering length density, with 5 Å interfacial roughness. This three-layer model gives a better fit than a two-layer model, and increasing the number of layers does not improve the quality of fit. Note that it is also possible to fit the reflectivity curves with other functional models. In our previous work, very detailed studies on adsorption of PNIPAM were carried out using protonated and deuterated polymers of different chain lengths and concentrations. The ensemble of these results permitted the reflectivity curves to be analyzed using power-law profiles.[41] In this study, our interest lies in the adsorption of nanoparticles, and for the curve obtained here, a three-layer model is found to give an adequate description of the reflectivity profile.

Table 1. Fitted Parameters for PNIPAM Adsorbed at the D_2O−Air Interface:[a]

	Nb 10^6 (Å^{-2})	ϕ_P	d (Å)	Γ (mg/m^2)	Γ^p (mg/m^2)
layer 1	0.95	0.99	3.4	0.36	0.65
layer 2	5.45	0.17	38.6	0.70	0.49
layer 3	6.30	0.02	115.2	0.25	1.78
			total	1.31	2.92

[a] Scattering length density (Nb), polymer volume fraction (ϕ_P), thickness (d), and total adsorption density (Γ). The last column (Γ^p) indicates the adsorption density of PNIPAM in the presence of 2% silica nanoparticles.

The corresponding fitted scattering length density profile is shown in Figure 1b. For PNIPAM alone, the layer nearest to the surface (layer 1) is very thin, $d = 3.4$ Å and Nb = 0.95 10^{-6} Å^{-2} which is very close to the Nb of pure polymer ($Nb_P = 0.90\ 10^{-6}$ Å^{-2}), indicating that this layer is rich in polymer. The second thicker layer, with Nb = 5.45 10^{-6} Å^{-2} is richer in solvent ($Nb_{D_2O} = 6.39\ 10^{-6}$ Å^{-2}), indicating a very dilute layer. Finally, the third layer, even thicker, is composed mostly of solvent. These results are very similar to those obtained in our previous studies using power-law profiles; they represent, respectively, the monomer-rich proximal zone, the fast-decaying central zone followed by an exponential tail.[41]

The volume fraction of polymer (ϕ_P) in each layer can be calculated from the relationships: $Nb_L = \phi_P Nb_P + \phi_{D_2O} Nb_{D_2O}$ and $\phi_P + \phi_{D_2O} = 1$, where Nb_L is the fitted scattering length density of the layer, and Nb_P and Nb_{D_2O} are scattering length densities of PNIPAM and D_2O, respectively. Taking the polymer density, $\rho = 1.07$ g/cm^3, the surface concentration in mg/m^2 can be evaluated from $\Gamma = \phi_P d\rho \times 10^{-1}$. The values obtained are 0.36 mg/m^2 in the first layer, 0.70 mg/m^2 in the second and 0.25 mg/m^2 in the third, giving a total adsorption density, $\Gamma = 1.31$ mg/m^2, a value that is coherent with previous results.[41] The fitted and calculated values for each layer are given in Table 1.

(ii) Silica Nanoparticles+PNIPAM. A dispersion of silica particles in pure water does not give any detectable adsorption at the water−air interface. In PNIPAM solution, however, the presence of particles in the interfacial region is indicated above particle concentration of 0.1% by weight. Figure 2 shows the

(41) Lee, L. T.; Jean, B.; Menelle, A. *Langmuir* **1999**, *15*, 3267.

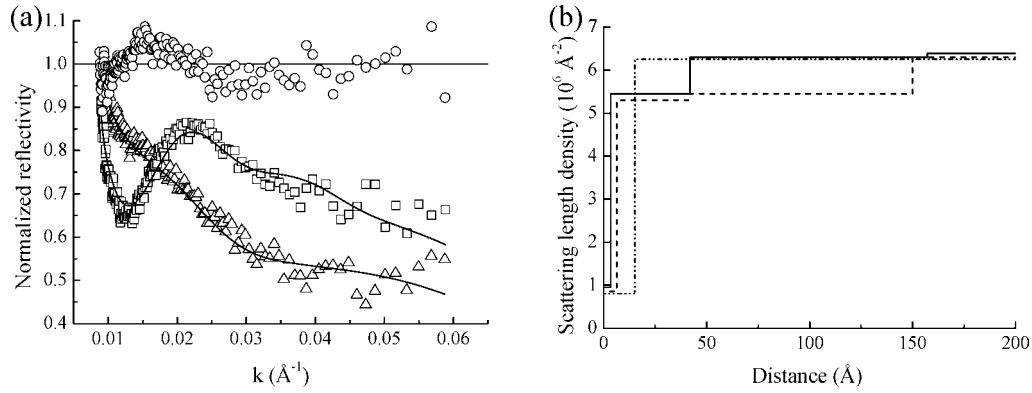

Figure 2. Silica nanoparticle adsorption from PNIPAM solution at the D_2O−air interface: (a) normalized reflectivity; PNIPAM only (triangles), PNIPAM+silica nanoparticles (squares), PNIPAM+SDS+silica nanoparticles (circles); $C_p = 10^{-3}$ g/mL, $C_s = 10^{-3}$ g/mL, $C_{particle} = 2\%$. The continuous lines are best-fit curves with corresponding scattering length density profiles shown in (b): PNIPAM only (solid line), PNIPAM+silica nanoparticles (dash line), PNIPAM+SDS+silica nanoparticles (dot-dash line). In this representation, $R/R_F < 1$ is attributed to total adsorbed layer.

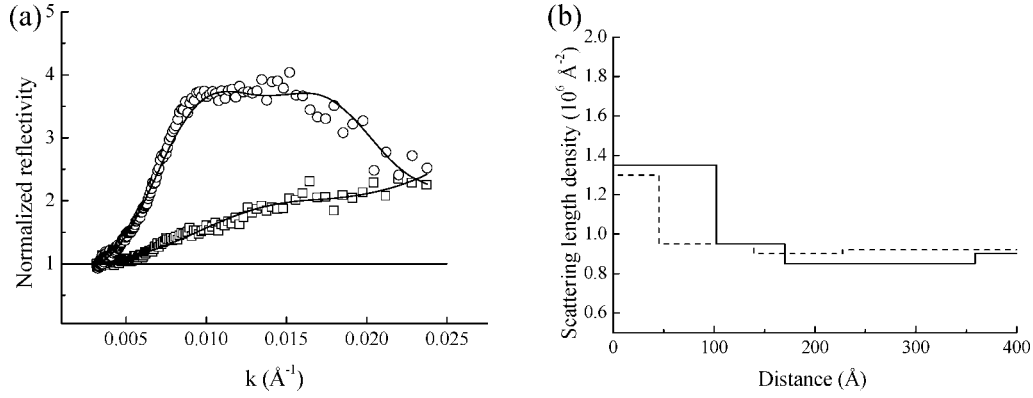

Figure 3. Effect of nanoparticle concentration on adsorption at the water−air interface; PNIPAM is contrast-matched to the solvent: (a) normalized reflectivity, $C_{particle} = 2\%$ (squares) and 4% (circles); $C_p = 10^{-3}$ g/mL. The continuous lines are best-fit curves with corresponding scattering length density profiles shown in (b): $C_{particle} = 2\%$ (dash line) and 4% (solid line). In this representation, $R/R_F > 1$ is attributed only to interfacial nanoparticles; a small depletion layer is also seen at the solution side.

reflectivity curve of a polymer solution containing 2% particles; here, the significant deviation from the pure polymer curve is evident. The solid lines are best-fit curves using a three-layer model with corresponding concentration profiles shown in Figure 2b. In the presence of SDS, the reflectivity curve is almost superimposed with the Fresnel (pure solvent) curve, represented here by $R/R_F \approx 1$. This result indicates that adsorption of the nanoparticles is completely depressed by SDS; this effect is studied in more detail in the next series of experiments.

Samples in Polymer Contrast-Matched Solvent. In the previous series of experiments, both polymer and nanoparticle contribute to the adsorption signal in the reflectivity curves. In this series, the polymer is contrast-matched to the solvent (D_2O/H_2O = 20:80 volume fraction). This solvent mixture has $Nb_s = 0.82 \times 10^{-6}$ Å^{-2}, which is exactly matched to that of PNIPAM, considering 20% exchangeable labile H with D in 20% D_2O. The reflectivity curve of PNIPAM in this solvent superposes with that of the pure solvent. In this contrast scheme, excess reflectivity signal is due only to the silica nanoparticles, and a precise concentration of particles at the interface can therefore be determined.

(i) Silica Nanoparticles+PNIPAM. Figure 3 shows reflectivity curves of nanoparticle dispersions at 2% and 4% bulk concentration where PNIPAM is contrast-matched to the solvent. Here, the contrast between particle and solvent is higher and positive, compared to the pure D_2O series ($\Delta Nb = Nb_{particle} - Nb_s = 3.96-0.82 \times 10^{-6}$ Å^{-2} = $+3.14 \times 10^{-6}$ Å^{-2}). The excess reflectivity due to adsorbed layer is consequently higher and positive, and $R/R_F > 1$. The high signals confirm significant nanoparticle adsorption at the free surface, and the adsorbed amount increases with particle concentration in the dispersion.

(ii) Silica Nanoparticles+PNIPAM+SDS. In this solvent, contribution from the protonated SDS is negligible. The presence of SDS decreases adsorption of the nanoparticles, an effect clearly seen in Figure 4 where R/R_F is decreased significantly. This reduction is observed for all nanoparticle concentrations up to 6%. At the fixed SDS concentration used in this study (C_s = 1 mg/mL), all particles are displaced from the surface when $C_{particle} < 2\%$; above this concentration, only partial displacement is obtained. For all samples containing SDS, a two-layer model is found to give the best fits to the experimental data.

An interesting feature revealed in this series is the presence of a depletion layer. This layer constitutes the third layer (in the three-layer model) or the second layer (in the two-layer model in the presence of SDS) situated below the nanoparticle layer on the solution side. This depletion layer is more evident in the presence of SDS provided the nanoparticles are not completely displaced.

The total surface concentration of silica nanoparticles is evaluated as mentioned previously. Since the polymer and surfactant do not contribute to the reflectivity signal, the sample can be considered, from the refractive index point of view, as a two-component system. Thus, the volume fraction of particle, $\phi_{particle}$, can be deduced from $Nb_L = \phi_{particle}Nb_{particle} + \phi_s Nb_s$ and

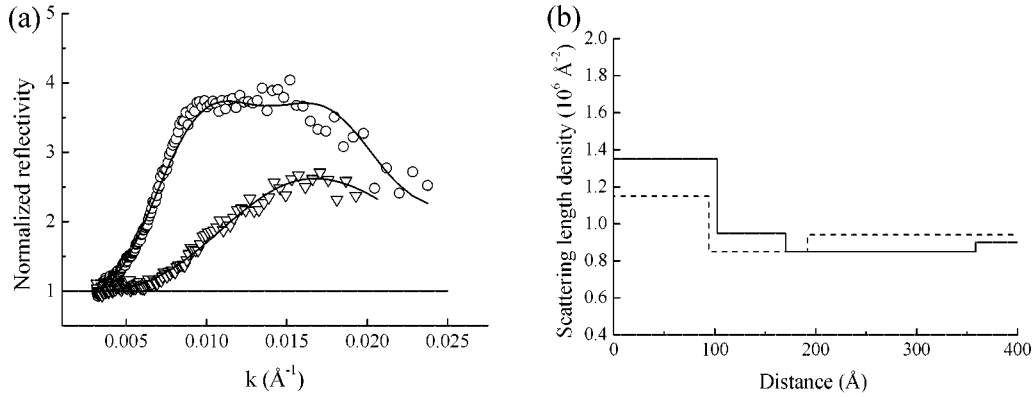

Figure 4. Effect of SDS on silica nanoparticle adsorption from PNIPAM solution at the water−air interface; PNIPAM is contrast-matched to the solvent: (a) normalized reflectivity in the absence (circles), and presence (inverted triangles) of SDS; $C_{particle} = 4\%$, $C_p = 10^{-3}$ g/mL, SDS concentration $C_s = 10^{-3}$ g/mL. The continuous lines are best-fit curves with corresponding scattering length density profiles shown in (b); $C_s = 0$ (solid line), $C_s = 10^{-3}$ g/mL (dash line). In this representation, $R/R_F > 1$ is attributed only to interfacial nanoparticles; a depletion layer is also evident at the solution side.

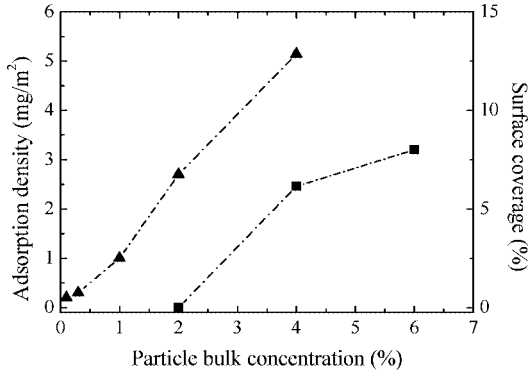

Figure 5. PNIPAM-activation adsorption of silica nanoparticles at the water−air interface in the absence of SDS (triangles), and in the presence of SDS (squares).

$\phi_{particle} + \phi_s = 1$, where ϕ_s is the volume fraction of the solvent containing the contrast-matched out polymer. From the value of $\phi_{particle}$ obtained from this series, the volume fraction of PNIPAM can be evaluated from the previous series of experiments in D_2O from, $Nb_L = \phi_p Nb_p + \phi_{particle} Nb_{particle} + \phi_{D_2O} Nb_{D_2O}$ and $\phi_p + \phi_{particle} + \phi_{D_2O} = 1$. Interestingly, it is found that in the presence of nanoparticles, the amount of PNIPAM at the interface is increased: at 2% nanoparticles, the adsorption density of PNIPAM is more than doubled, from 1.31 to 2.92 mg/m^2 (see Table 1). This information supports the notion that the nanoparticles adsorb at the interface by virtue of a coating of the amphiphilic polymer.

Figure 5 shows nanoparticle adsorption as a function of bulk concentration in the presence of PNIPAM and SDS. Two aspects are noted, (i) the particle adsorption density increases with bulk concentration and (ii) this adsorption is reduced 2−3-fold in the presence of SDS.

Adsorption at Hydrophilic Surface (Oxidized Silicon−Water Interface). For adsorption studies at a hydrophilic interface, a system of silicon wafer with a layer of oxidized SiO_2 (∼22 Å) and D_2O is used. Reflectivity at this interface for a solution of PNIPAM does not differ significantly from that of the pure solvent, indicating only minimal polymer adsorption at this interface. Due to the low signal from the polymer, the fitted parameters can be considered only to give estimated values: $d \approx 30$ Å, $\phi_p \approx 0.1$ giving $\Gamma \approx 0.3$ mg/m^2, with the polymer adsorbed in a flat conformation. In the presence of nanoparticles, only small changes are obtained in this layer; on the other hand, a small depletion layer about the size of the adsorbed layer, is detected (Figure 6). It can thus be concluded that nanoparticle adsorption at this surface is negligible.

Discussion

PNIPAM Adsorption at Interfaces. Due to its partially hydrophobic character, PNIPAM adsorbs spontaneously at the air−water interface. The three-layer adsorption model used to describe the adsorbed layer at the apolar air interface at 20 °C indicates a molecularly thin and almost pure polymer followed by two increasingly more dilute layers. The total thickness of the adsorbed layer, $d \approx 150$ Å is of the order of the radius of gyration of the polymer. The total adsorption density, $\Gamma = 1.31$ mg/m^2 agrees with typical values obtained for adsorption of neutral homopolymer in good solvents (surface concentration between 1 and 2 mg/m^2). All of these characteristics are consistent with our previous analyses using a power-law model.[41]

Silica Nanoparticle−PNIPAM Interaction. On a hydrophilic (macroscopic silica) surface, the preponderance of PNIPAM to adsorb is decreased 4−5-fold. In spite of the low interaction with macroscopic silica surface, PNIPAM nevertheless associates strongly with negatively charged silica nanoparticles. That PNIPAM adsorbs onto silica nanoparticles has already been reported by other groups[42] and also by our past work using electron-loss spectroscopy elemental mapping. These images provide direct evidence of adsorbed polymer layer around the nanoparticles.[43] For this system, the most commonly cited driving force is H-bonding. However, our microscopy studies show that despite its globally charged and hydrophilic nature, the microchemistry of silica nanoparticle exhibits surface inhomogeneities that include hydrophobic domains.[44] These domains favor interactions with an amphiphile, as in the case of PNIPAM. We propose therefore, that hydrophobic interaction contributes an additional driving force for PNIPAM−silica nanoparticle associations.

Silica Nanoparticle Adsorption at Interfaces: Modulation by PNIPAM and SDS. While detailed studies of PNIPAM adsorption at interfaces have been reported previously, this is the first report to our knowledge concerning silica nanoparticle adsorption behavior at both hydrophobic and hydrophilic

(42) Petit, L.; Bouteiller, L.; Brulet, A.; Lafuma, F.; Hourdet, D. *Langmuir* **2007**, *23*, 147.
(43) Costa, C. A. R.; Leite, C. A. P.; Lee, L. T.; Galembeck, F. *Prog. Colloid Polym. Sci.* **2004**, *128*, 74.
(44) Costa, C. A. R.; Leite, C. A. P.; Galembeck, F. *J. Phys. Chem. B* **2003**, *107*, 4747.

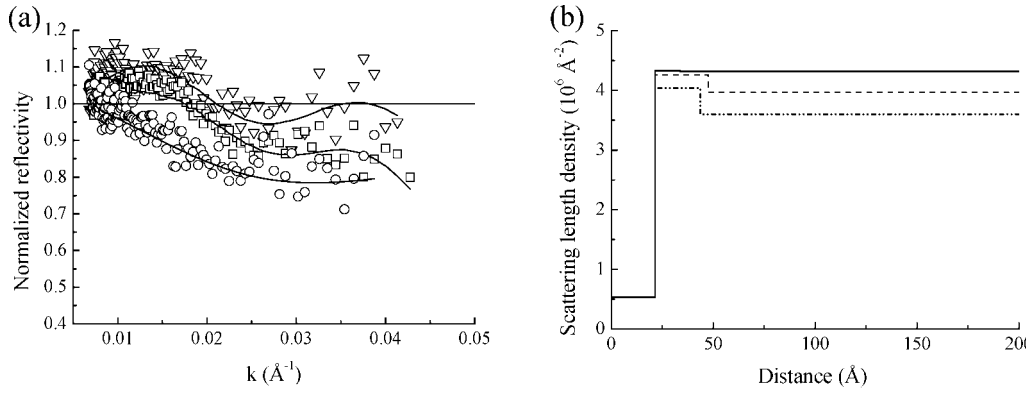

Figure 6. Normalized reflectivity of silicon−liquid interface: PNIPAM solution in D_2O without nanoparticles (circles)—this curve is very close to the silicon−D_2O curve; PNIPAM+silica nanoparticles at $C_{particle} = 2\%$ (squares) and 6% (inverted triangles); $C_p = 10^{-3}$ g/mL. Fitted scattering length density profiles (b): PNIPAM/D_2O (very close to pure D_2O curve) (solid line), $C_{particle} = 2\%$ (dash line) and 6% (dot-dash line). In this system, a big contribution to the R/R_F signal arises from the oxidized silica layer (22 Å). The results show insignificant amount of nanoparticles at the interface and a small depletion layer.

Table 2. Particle Size and Zeta-Potential Values of Silica Nanoparticles in PNIPAM and SDS Solutions

sample	particle size (diameter)/nm	ξ potential (mV)	mobility (μm/s·V·cm)
silica alone	63.0 ± 0.4	−36.8 ± 2.0	−2.88 ± 0.16
silica + PNIPAM	101.7 ± 1.5	−10.4 ± 1.8	−0.82 ± 0.14
silica + SDS	66.7 ± 0.6	−36.0 ± 1.1	−2.81 ± 0.08
silica + PNIPAM + SDS	93.4 ± 0.5	−28.6 ± 1.1	−2.34 ± 0.09

interfaces. Adsorption of the nanoparticle is driven by its interaction with PNIPAM in solution, and by the interfacial properties of PNIPAM. These solution and surface properties are modulated in the presence of SDS.[45]

Adsorption of PNIPAM on the silica nanoparticles produces two effects: it renders the particle surface-active, and it reduces the surface charge potential. In this case, the zeta potential of the nanoparticle is decreased from ∼ −40 to ∼ −10 mV in the presence of the adsorbed layer (see Table 2). Consequently, at a hydrophobic surface where bare silica nanoparticle attraction is not detected, surface modification by the PNIPAM coat activates its adsorption. Interestingly, a synergistic enhancement of PNIPAM adsorption by the nanoparticles is also observed. On a hydrophilic (silica) surface, in spite of the reduced electrostatic repulsion, no detectable nanoparticle adsorption to the silica surface is found. These different tendencies are a consequence of the adsorption behavior of the polymer: strong at hydrophobic and weak at hydrophilic interface (Figure 7).

The presence of SDS suppresses adsorption of the nanoparticles. At low particle concentration, the particles are completely displaced from the surface. This behavior is related to bulk interaction of SDS with PNIPAM forming charged chains with a "necklace" structure, with each chain consisting of several bound SDS micelles.[46] Our past studies have already shown displacement of adsorbed PNIPAM from the water−air interface by SDS; furthermore, adsorption of the charged chains to the hydrophobic interface is thermodynamically unfavorable. The resultant surface layer consists of a thin mixed layer of polymer and surfactant.

PNIPAM−SDS association thus competes with PNIPAM–nanoparticle interaction. The question then arises as to whether one or two different populations of chains are formed: one type of chain containing polymer−surfactant−nanoparticle or a mixture of chains each type containing exclusively micelles or charged nanoparticles. For this system, the zeta potential of the nanoparticle increases to ∼ −29 mV indicating coadsorption of polymer and surfactant or displacement of PNIPAM from the nanoparticle surface. Inspection of the values of zeta potential and of the hydrodynamic radius, with respect to the bare particles, suggests partial displacement of the adsorbed PNIPAM with coadsorption of the SDS molecules. This interpretation is supported by microscopy elemental map imaging that shows accumulations of carbon and sodium around the nanoparticles. Since the sodium arises principally from the SDS, these images provide direct evidence for PNIPAM−SDS−silica nanoparticle associations (Figure 8). A detailed study on elemental map distributions of the PNIPAM−silica system has been reported previously.[43]

Thus, coadsorption and recharging of the nanoparticle by SDS depresses or deactivates its interfacial activity. An interesting feature revealed by the nanoparticle concentration profile is the depletion zone between the adsorbed layer and the bulk concentration, indicating repulsion between adsorbed and bulk species. Formation of a mixed layer of polymer−nanoparticle−SDS on the hydrophobic surface thus transforms it into a hydrophilic one. Consequently, further build-up to form a thick nanoparticle multilayer is prevented.

Silica Nanoparticle Adsorption at Interfaces: Consequences on 2-D Organization. Adsorption behavior of nanoparticles obtained in this study can be related to previous observations on controlled organization of nanoparticles on solid substrates using polymer−surfactant solutions. This method involves two basic ideas: particle self-assembly and dewetting behavior of the thin liquid film. Self-assembly of particles occurs by a two-stage mechanism:[47] (i) nucleation of an ordered phase by lateral capillary attractions when the liquid level falls below the particle size and (ii) convective transport of particles toward the ordered region. A dispersion of nanoparticles in pure water deposited on a substrate thus forms self-assembled close-packed domains. Dewetting behavior is controlled by the physicochemistry of the solution and on the nature of the solid substrate; for PNIPAM−SDS solutions, dewetting patterns can be tuned to form polygonal and long-chain morphologies. Our approach employs these complex dewetting patterns to template the particle nucleation step, by confining the particles within the dewetting liquid film morphologies. Lateral capillary attractions of the confined particles thus form structures according to the dewet patterns.

(45) Jean, B.; Lee, L. T.; Cabane, B. *Langmuir* **1999**, *15*, 7585.
(46) Lee, L. T.; Cabane, B. *Macromolecules* **1997**, *30*, 6559.
(47) Denkov, N. D.; Velev, O. D.; Kralchevsky, P. A.; Ivanov, I. B.; Yoshimura, H.; Nagayama, K. *Langmuir* **1992**, *8*, 3183.

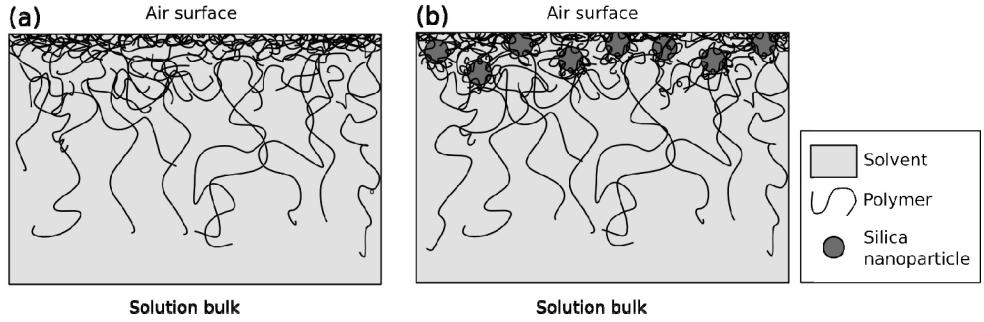

Figure 7. Schematic drawing of polymer and polymer-activated nanoparticle adsorption at the air−water interface.

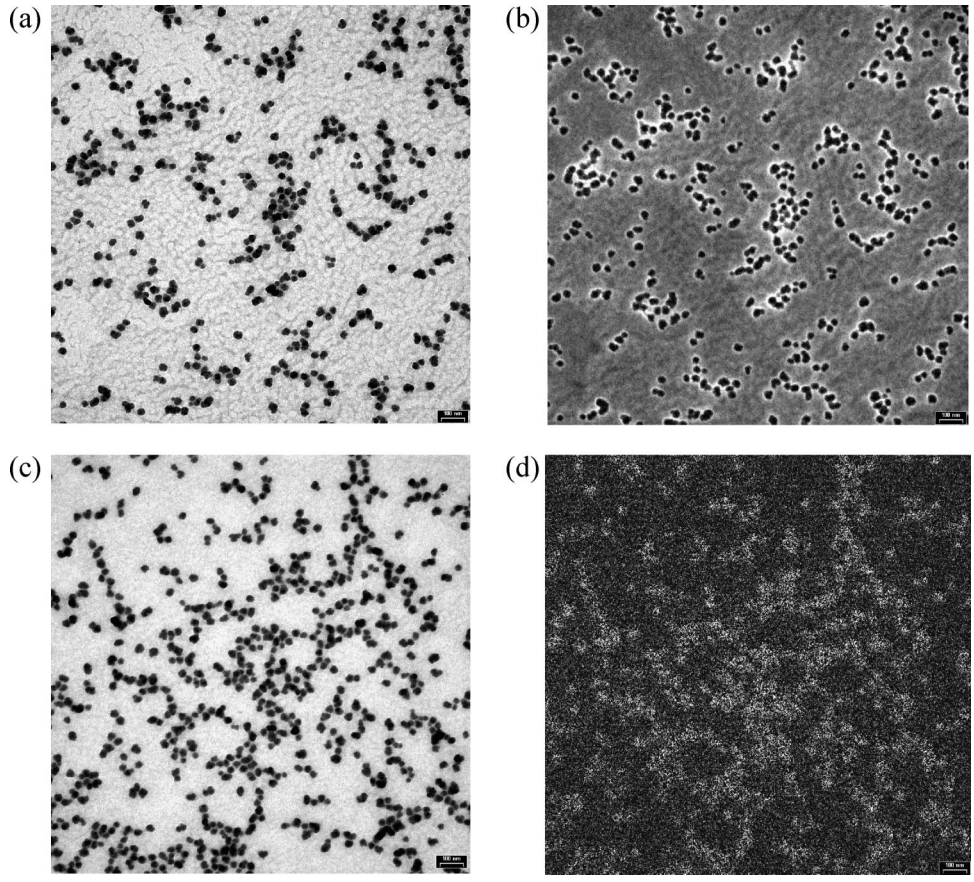

Figure 8. TEM images of a dry dispersion of silica nanoparticles in PNIPAM−SDS solution: Bright field (a) and carbon map (b); bright field (c) and sodium map (d).

Using this approach, we have found that controlled organization depends on the substrate−observations that can now be related to effects of particle−substrate adhesion. On a hydrophilic substrate (mica), minimal attractive or repulsive particle−substrate interaction allows the nanoparticles to be dragged and confined by the dewetting liquid which, upon drying form polygonal network and long-chain structures, as templated according to the dewetting film morphologies (Figure 9).

On a hydrophobic surface (graphite), however, this approach fails. Aggregates of nanoparticles are deposited onto the substrate without features of dewetting morphology (Figure 10). Here, particle−substrate attraction impedes the particle mobility, preventing the particles from being dragged by the receding edge of the dewetting film. Note that particle adhesion to substrate affects only the confinement and convective stages of the liquid template method. The nucleus formation stage remains mostly unaffected by adhesion forces since, for neighboring particles whose menisci overlap, the attractive lateral capillary force is calculated to be of the order of 10^4 kT for particles of about 100 nm,[47] several orders of magnitude larger than adsorption forces. This large capillary force explains the inevitable occurrence of some degree of two-dimensional aggregates, irrespective of physicochemical properties of the nanoparticle system. Indeed, the image in Figure 10 shows a monolayer of small islands of nanoparticles covering the hydrophobic substrate, over which are deposited large aggregates of the nanoparticles. This feature can further be related to the depletion layer revealed in the adsorption profile that indicates repulsion of adsorbed and bulk species. The adsorbed polymer−SDS−nanoparticle mixed layer on the hydrophobic surface thus transforms it into a hydrophilic one. Consequently, further build-up to form a thick nanoparticle multilayer is prevented. The remaining nanoparticles in the liquid film, prevented from further adsorption, coupled with poor liquid spreading, aggregate as the concentration increases during subsequent evaporation and are deposited on the monolayer-coated substrate.

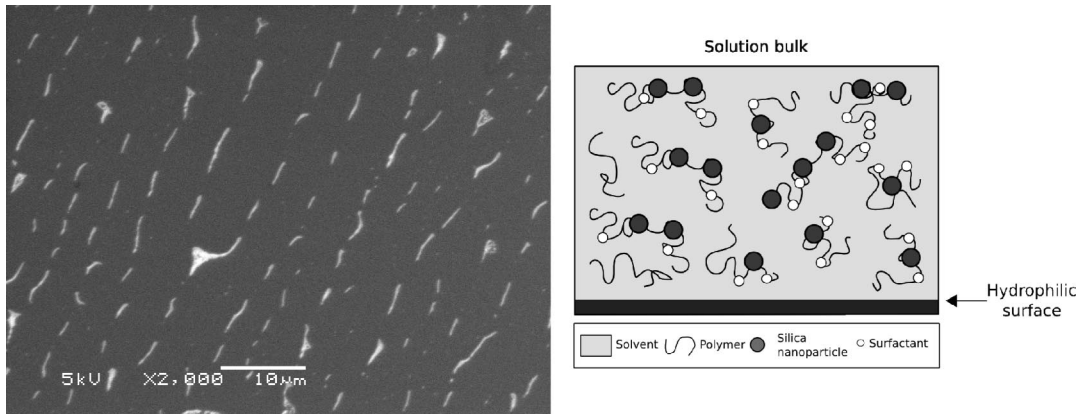

Figure 9. Organized morphology of silica nanoparticles templated by dewetting of PNIPAM−SDS solution ($C_s/C_p = 1$) on a hydrophilic substrate (mica). Absence of particle adhesion to the substrate favors the pattern formation.

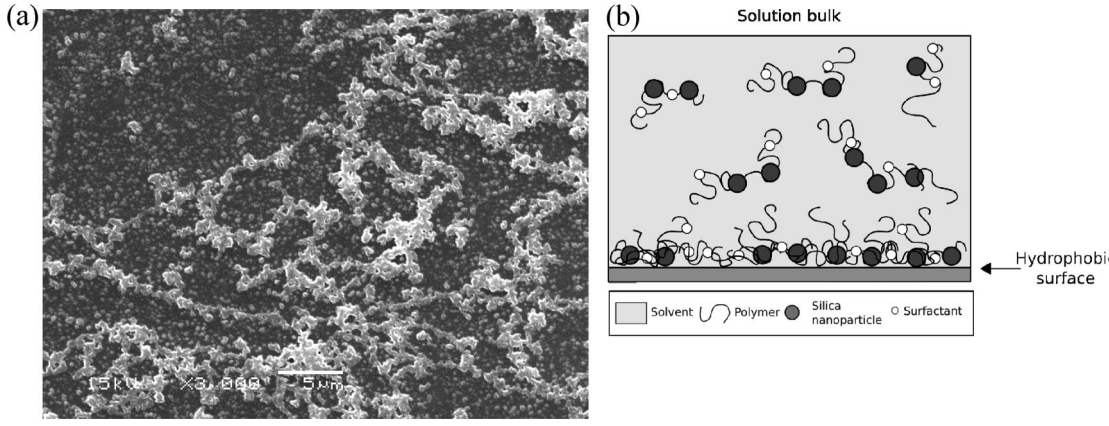

Figure 10. SEM micrograph of silica nanoparticles in PNIPAM−SDS solution ($C_s/C_p = 1$) deposited on a hydrophobic substrate (graphite). No features of the liquid-dewetting template are observed due to particle−substrate interaction.

Conclusions

Silica nanoparticles at hydrophobic and hydrophilic interfaces, as studied by neutron reflectivity, show a wide range of interfacial behavior that is modulated by amphiphilic polymer PNIPAM and anionic surfactant SDS. While the negatively charged nanoparticle does not show attraction to either surface, its interaction with PNIPAM activates its adsorption at the hydrophobic one. SDS competes with nanoparticle in its interaction with PNIPAM. The results of this study indicate coadsorption of PNIPAM and SDS on the nanoparticle, resulting in complete suppression or significant reduction in adsorption. Interestingly, a depletion layer is formed due to repulsion between adsorbed and bulk species. This repulsion prevents formation of a thick multilayer.

These adsorption results attest to the importance of particle–substrate interaction in the control of nanoparticle self-assembly using liquid dewetting templates. In the absence of significant particle−substrate attraction (hydrophilic substrate), the nanoparticles are dragged and confined within the dewetting liquid and organize according to the liquid dewetting patterns that include polygonal and long-chain structures. On the other hand, adhesion of particle to substrate (hydrophobic surface) impedes this lateral movement and the template process fails. In this case, the nanoparticles form islands and aggregates resulting in dry morphologies devoid of the liquid template features.

Acknowledgment. C.A.R. and F.G. thank FAPESP, CAPES, and CNPQ for financial support. We also thank F. Cousin and A. Menelle for help on the reflectometer.

LA8004807